Interaction of the Complexin Accessory Helix with the C-Terminus of the SNARE Complex: Molecular-Dynamics Model of the Fusion Clamp

Maria Bykhovskaia,[†*] Anand Jagota,[‡§] Agustin Gonzalez,[†] Alexander Vasin,[†] and J. Troy Littleton[¶‖††]
[†]Neuroscience Department, Universidad Central del Caribe, Bayamon, Puerto Rico; [‡]Department of Chemical Engineering and [§]Bioengineering Program, Lehigh University, Bethlehem, Pennsylvania; and [¶]Picower Institute for Learning and Memory, [‖]Department of Biology, and [††]Department of Brain and Cognitive Sciences, Massachusetts Institute of Technology, Cambridge, Massachusetts

ABSTRACT SNARE complexes form between the synaptic vesicle protein synaptobrevin and the plasma membrane proteins syntaxin and SNAP25 to drive membrane fusion. A cytosolic protein, complexin (Cpx), binds to the SNARE bundle, and its accessory helix (AH) functions to clamp synaptic vesicle fusion. We performed molecular-dynamics simulations of the SNARE/Cpx complex and discovered that at equilibrium the Cpx AH forms tight links with both synaptobrevin and SNAP25. To simulate the effect of electrostatic repulsion between vesicle and membrane on the SNARE complex, we calculated the electrostatic force and performed simulations with an external force applied to synaptobrevin. We found that the partially unzipped state of the SNARE bundle can be stabilized by interactions with the Cpx AH, suggesting a simple mechanistic explanation for the role of Cpx in fusion clamping. To test this model, we performed experimental and computational characterizations of the *syx*$^{3\text{-}69}$ *Drosophila* mutant, which has a point mutation in syntaxin that causes increased spontaneous fusion. We found that this mutation disrupts the interaction of the Cpx AH with synaptobrevin, partially imitating the *cpx* null phenotype. Our results support a model in which the Cpx AH clamps fusion by binding to the synaptobrevin C-terminus, thus preventing full SNARE zippering.

INTRODUCTION

Release of neurotransmitters from nerve terminals is dynamic, plastic, and highly regulated. Synaptic vesicles dock at presynaptic active zones, fuse with the plasma membrane, and release transmitters into the synaptic cleft. Vesicle docking is mediated by the SNARE complex, which forms as a parallel four-helix bundle comprising the vesicle transmembrane protein synaptobrevin (Syb), the plasma membrane protein syntaxin (Syx), and the membrane-anchored protein SNAP25. The SNARE-binding protein synaptotagmin (Syt) serves as a Ca^{2+} sensor and triggers vesicle fusion in response to an action potential. Action-potential-evoked fusion events are very rapid and highly synchronized in time. Therefore, it has been hypothesized that fusion of release-ready vesicles may be prevented or clamped in anticipation of an action potential, and that this clamp dynamically regulates the fusion machinery. Such a role in fusion clamping has been ascribed to the small cytosolic protein complexin (Cpx) (1–6).

Numerous studies have suggested that Cpx acts both to inhibit spontaneous neurotransmitter release in the absence of Ca^{2+} (1–3,7,8) and to promote evoked neurotransmitter release (1–3,7–11). Data from biochemical studies (12,13), genetic knockout studies in *Drosophila* and *Caenorhabditis elegans* (1,2,7,8) and genetic knockdown studies in mice (3) have supported the role of Cpx as an inhibitor of spontaneous neurotransmitter release. Genetic deletion of the single Cpx homolog in *Drosophila* results in a dramatic increase in the frequency of spontaneous vesicle fusion events (minis) at the larval neuromuscular junction (NMJ) (1,2,4). Similarly, the frequency of tonic fusion events at the *C. elegans* NMJ is increased in genetic knockouts of the primary Cpx homolog (7,8). Unlike flies and worms, mammals have four Cpx genes with distinct expression patterns in the nervous system (14). RNAi knockdown of Cpxs in mouse cortical cultures was shown to increase spontaneous neurotransmitter release (3). However, genetic knockout of Cpxs resulted in decreased spontaneous neurotransmitter release at hippocampal autapses and GABA-/glycinergic synapses, but not at striatal autapses (10,15,16). In contrast to the different findings on spontaneous fusion, studies have consistently shown that Cpx is necessary to promote evoked Ca^{2+}-dependent neurotransmitter release (1–3,7–11,15,17). These data indicate that Cpx has distinct effects on different modes of neurotransmitter release and plays several roles during the multistep process of synaptic vesicle fusion.

Although extensive and compelling evidence supports a clamping function of Cpx, it remains obscure how Cpx specifically clamps vesicle fusion, and what state of the SNARE complex corresponds to the fusion clamp. Cpx contains a central α-helix (CH) that binds tightly to the SNARE bundle (18) and is required for Cpx to function (3). In addition, Cpx contains an N-terminal accessory helix (AH) positioned in the vicinity of the SNARE bundle C-terminus, although combined x-ray and NMR analyses suggested that the Cpx AH does not interact with the SNARE bundle (18). Site-directed mutagenesis coupled with functional analysis at hippocampal synapses suggested that the clamped prefusion state corresponds to a partially assembled SNARE complex, and that the Cpx AH prevents full zipping of the four-helix SNARE bundle (19). Other studies supported this

Submitted March 13, 2013, and accepted for publication June 14, 2013.

*Correspondence: mb.ucdelcaribe@gmail.com

Editor: Scott Feller.

0006-3495/13/08/0679/12 $2.00

http://dx.doi.org/10.1016/j.bpj.2013.06.018

hypothesis, demonstrating that destabilizing the C-terminus of the SNARE bundle may clamp spontaneous fusion (20,21). An early model of the fusion clamp proposed that the Cpx AH competes with Syb for binding to the SNARE complex (5), and a biochemical study (22) demonstrated that the truncated Cpx AH can potentially displace the C-terminus Syb motif. The latter study, however, also demonstrated that this is not the case when the Cpx N-terminal region is present, which diminishes the likelihood that such a mechanism regulates fusion in vivo. A subsequent study (6) included x-ray analysis of the SNARE bundle with truncated Syb C-terminus and in a complex with mutated Cpx. This study demonstrated that when the C-terminus Syb motif is truncated, the mutated Cpx can bind to the SNARE complex in lieu of the missing Syb N-terminus domain, thus cross-linking two different SNARE complexes. It was thus suggested that several cross-linked SNARE complexes produce the clamped and fusion-incompetent vesicle state. However, this model involves a radical unzipping of the SNARE bundle and substantial bending of the Syb helical domain, which is likely to entail a high energetic cost. Therefore, it was also proposed (23) that the SNARE bundle acts as a single-shot device that completes assembly in an unstoppable manner once N-terminal zipping is triggered.

Thus, it remains obscure how Cpx clamps vesicle fusion in vivo. To analyze this mechanism, to explore molecular models of the fusion clamp, and to evaluate their energetic costs, we performed molecular-dynamics (MD) simulations of the SNARE complex bound to Cpx. Although MD simulations of the SNARE complex without (24–26) and with (27) Cpx have been performed, and the overall flexibility of the SNARE bundle has been evaluated, the stability of the SNARE bundle C-terminus has not been explored in detail. In this study, we performed a computational imitation of the forces exerted by membrane and vesicle on the SNARE bundle. To accomplish this, we evaluated the electrostatic repulsion between the vesicle and the membrane, and performed MD simulations of the SNARE/Cpx complex under external forces. The results of our simulations suggest that the clamped state of the SNARE complex may correspond to a separation of the two C-terminus layers, but is unlikely to involve a more radical unzipping. Furthermore, we discovered that binding of the Cpx AH to the SNARE C-terminus has a destabilizing effect without displacing Syb, favoring a partially unzipped state of the SNARE C-terminus. Thus, we describe here a parsimonious, energetically favorable model of the fusion clamp. This model also explains the *cpx*-like phenotype observed in the *Drosophila* temperature-sensitive (TS) paralytic mutant $syx^{3\text{-}69}$ (28,29).

MATERIALS AND METHODS

Molecular modeling

For the initial topology of the SNARE complex, we used the high-resolution (1.4A) x-ray structure 1N7S (30). The structure was optimized based on the Monte-Carlo minimization (MCM) approach (31), employing the ZMM/MVM software package (www.smmsoft.com (32)). The optimized topology did not deviate substantially from the 1N7S structure.

The initial topology of the SNARE/Cpx complex was constructed out of two x-ray structures: 1N7S, the high-resolution structure of the SNARE complex, and 1KIL (18), the structure of the SNARE/Cpx complex obtained by a combination of crystallography and NMR approaches with 2.3 Å resolution. The SNARE/Cpx model was constructed with the use of the ZMM/MVM package as follows: 1), with the SNARE bundle geometry (from 1N7S) and Cpx geometry (from 1KIL) kept rigid, docking was performed by imposing harmonic distance constraints (obtained from 1KIL SNARE/Cpx structure) on all of the interacting atoms of the SNARE bundle and Cpx; 2), the resulting structure was optimized by MCM imposing constraints on all the Cα atoms, which were rigidly pinned; and 3), the resulting structure was optimized employing MCM with no constraints.

MD computations were performed with the use of NAMD Scalable Molecular Dynamics (33) and VMD Visual Molecular Dynamics Software (Theoretical and Computational Biophysics Group, NIH Center for Macromolecular Modeling and Bioinformatics, Beckman Institute, University of Illinois at Urbana-Champaign). The CHARMM22 force field (All-Hydrogen Parameter File for Proteins with CMAP correction (34)) was used. The single-point mutation in the Syx protein was performed with the use of VMD software. The water box (150 $\times$ 70 $\times$ 70 Å) was constructed using VMD, and potassium and chloride ions were added to neutralize the negative charge of the protein complex and to yield a 150 mM concentration of KCl.

For the MD computations we employed NAMD with periodic boundary conditions and Ewald electrostatics at a constant pressure (Berendsen barostat). The bond length of water molecules were constrained with the use of the SHAKE algorithm. A brief energy minimization was followed by a 10 ps heating phase, a 100 ps equilibration phase, and subsequent production runs at 300 K temperature (Langevin thermostat with a coupling coefficient of 5 ps^{-1}) with a 2 fs step. For simulations under external forces, we used a time step of 1 fs in combination with temperature rescaling to ensure stability. Computations were performed either at the University of Puerto Rico High Performance Computing Facility or at Extreme Science and Engineering Discovery Environment resources (National Institute of Computational Science and Texas Advanced Computing Center).

Electrophysiology

We used the following fly stocks: Canton-S (wild-type (WT); Bloomington *Drosophila* Stock Center), *cpx* null mutant cpx^{SH1} (1), and syntaxin *TS* $syx^{3\text{-}69}$ mutant (28). Experiments were performed on type Ib boutons (35) of muscles 6 and 7 at abdominal segments 2, 3, and 4 of the third instar larvae in HL3 solution (36), containing (in mM) 70 NaCl, 5 KCl, 1 $CaCl_2$, 20 $MgCl_2$, 10 $NaHCO_3$, 5 trehalose, 115 sucrose, and 5 HEPES. Synaptic responses were recorded focally as previously described (37,38) from boutons visualized with DIC optics using macropatch electrodes of 5–10 μm tip diameter. The electrodes were manually bent to enable recordings under a 60$\times$ magnification water immersion objective (Olympus, 0.95 NA) with a 2 mm working distance. Recordings were digitized with a Digidata A/D board and Axoscope software (Axon Instruments), and analyzed offline with in-house-developed Quantan software (39).

RESULTS

The Cpx AH forms a tight complex with the SNARE bundle in a water-ion environment

To begin our analysis, we optimized the SNARE/Cpx structure by employing the MCM approach. The energetically optimal conformation did not differ substantially (root mean-square deviation (RMSD) = 2.08 A) from the

initial x-ray structure (Fig. 1 *A*). However, the Cpx AH was in tighter contact with the SNARE bundle, with the Cpx AH interacting with Syb. To investigate the stability of this conformation, we performed a 250 ns MD simulation of the SNARE/Cpx complex in a water-ion environment. The resulting structure had even tighter contacts between Cpx and the SNARE bundle, including both the CH and AH (Fig. 1, *A* and *B*). In this final structure, the Cpx AH was positioned in the groove between Syb and the C-terminal domain of the SNAP25 (SN2), and was stabilized by salt bridges and hydrophobic interactions with both proteins (Fig. 1 *B*).

We next analyzed the entire MD trajectory, focusing on the interactions between Cpx and Syb, and between Cpx and SN2 (Fig. 1 *C*). The initial 20 ns of the simulation were characterized by frequent dissociations of the Cpx AH from Syb (Fig. 1 *C*, *black line*), whereas contacts between Cpx AH and SN2 were not yet formed (Fig. 1 *C*, *red line*). During a subsequent 20 ns simulation, the structure remained stable, with the Cpx AH being in tight contact with Syb. Finally, after a 40 ns simulation, a conformation transition occurred, and the Cpx AH moved into the groove between Syb and SN2, being stabilized by salt bridges and hydrophobic interactions with both proteins. This structure proved to be stable and remained intact for 170 ns of the MD simulation, with only brief and infrequent breakages of one of the stabilizing salt bridges (Fig. 1 *C*).

Thus, we found that in the water-ion environment, the Cpx AH is likely to form close contacts with the SNARE bundle. We questioned whether this could account for the effect of the Cpx AH on the stability of the SNARE C-terminus, and for the role of the Cpx AH in fusion clamping. For the initial evaluation of the stability of the SNARE C-terminus, we examined the fluctuations of the distance between the Cα atoms of the terminal residues of Syb (W89) and Syx (K256). We found that the C-terminus was stable (Fig. 1 *D*) and the distance fluctuations did not depend on the Cpx conformational state or the presence of Cpx. It should be noted, however, that this computation does not reflect the fact that the SNARE bundle is not isolated in vivo, and that its stability is influenced by its interaction with the vesicle and membrane. More specifically, the Syx and Syb transmembrane domains are anchored at their C-termini to the membrane and vesicle, respectively, and the two membranes are polarized. Thus, tension is exerted upon the SNARE C-terminus due to the repulsive electrostatic forces between the membrane and the vesicle. We next analyzed how strong the forces would have to be to partially unzip the SNARE C-terminus, how unzipping would depend on the force applied, and how Cpx would influence this process.

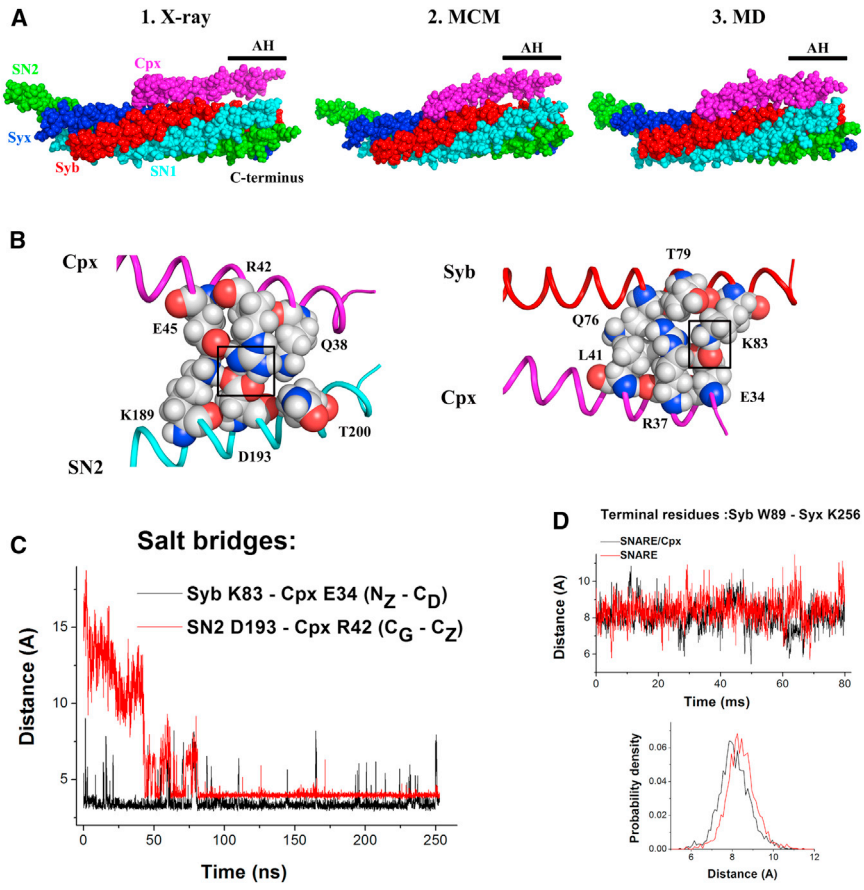

FIGURE 1 The Cpx AH comes into close contact with the SNARE bundle, and this conformation is stabilized by salt bridges between Cpx and Syb, and between Cpx and SN2. (*A*) Conformations of the SNARE complex with Cpx obtained by x-ray (1KIL), after MCM optimization, and at the end of the 250 ns MD trajectory. The AH makes close contact with the SNARE bundle (Syb, *red*; Syx, *blue*; SN1, *green*; SN2, *cyan*; Cpx, *magenta*). (*B*) Stabilizing interactions of Cpx with SN2 and Cpx. Boxes indicate stable salt bridges. (*C*) MD trajectory of the Cpx/SNARE complex, showing a formation of stable salt bridges between Cpx and Syb (*black*) and Cpx and SN2 (*red*). (*D*) Fluctuations of the C-terminal residues of the SNARE complex do not depend on the presence of Cpx. The final 80 ns of the SNARE/Cpx trajectory (*black*) are compared with 80 ns simulation of the SNARE complex alone (*red*). The distance between the Cα atoms of W89 of Syb and K256 of Syx is plotted.

Electrostatic repulsion between the vesicle and plasma membrane

We estimated the electrostatic repulsion of the vesicle and synaptic membranes. This repulsion is balanced by opposing tensile forces on the C-termini of Syb and Syx that could partially unzip the SNARE complex. To calculate this force, we considered two polarized planes (the vesicle and the membrane) carrying different surface potentials (Supporting Material, part 1). The electrostatic potential was calculated using the Debye-Huckel equation, which is a linearized version of the nonlinear Poisson-Boltzmann equation (40,41) (Supporting Material, Eqs. S1 and S2). To calculate the electrostatic force between the vesicle and the membrane, we had to make an assumption about the relationship between the surface potential and surface charge. We considered two limiting cases (40):

1. The surface potential is fixed and the surface charge adjusts to keep it at a constant level. The surface charge could adjust to compensate for the potential change either via redistribution of ions, such as K^+, in the vicinity of the membrane, or via polar lipid groups adjusting their degree of ionization. Both mechanisms would work to minimize the change in the surface potential.
2. The surface charge is fixed and the surface potential adjusts. This is the limiting case corresponding to fully ionized groups with a fixed charge.

The actual situation is far from trivial, since ionizable groups that produce polarization of both vesicle and plasma membrane may adjust their charges. The electrostatic interaction between the vesicle and the membrane lies between these two extreme limits and corresponds to charge regulation (40), where ion redistribution and changes in ionization of lipid polar groups only partially compensate for the increase in the surface potential that occurs when the membrane and the vesicle come into closer contact. Thus, force estimates in these limits determine the bounds for the electrostatic repulsive force between the vesicle and the membrane.

Let us consider the first case, in which the potential is specified and fixed on both surfaces. Here it can be shown that the repulsive force between the vesicle and the membrane remains finite and its maximum value can be described by Eq. S10 in the Supporting Material (part 1). Using parameters provided in Table S1, we obtain a value of maximum force equal to 93 pN (1.3 kcal/mol/Å, which equals approximately two times the thermal fluctuation energy per angstrom, 2 k_BT/Å). This is a lower estimate of the electrostatic repulsion because it is calculated under an assumption that ions and ionic groups will fully compensate for an increase in the surface potential produced by shortening the distance between the vesicle and the membrane. In reality, this compensation is likely to be only partial, and this would increase the force.

Let us now consider the case in which the surface charge is held fixed. In this case, it can be shown (Supporting Material, part 1, Fixed Charge) that the repulsive force between the vesicle and the membrane is described by Eq. S15. Using the parameter values provided in Table S1 and taking the distance between the vesicle and the membrane to be equal to 1 nm, which approximately equals the distance between the Syb and Syx C-terminal residues in the fully assembled SNARE bundle, we estimate the repulsive force to be 210 pN, which is approximately five times the thermal fluctuation energy k_BT/Å. Clearly, this is an upper estimate of the repulsive force, since at least partial charge compensation would occur in a media containing ions, and this compensation will reduce the electrostatic field. Based on these calculations, we estimate that when a vesicle is docked to the membrane by a single SNARE complex that is fully assembled, a repulsive electrostatic force ranging from 90 to 210 pN will be exerted and directed to separate the bundle.

Notably, the difference between the fixed potential and fixed charge calculations is significant only when the vesicle and membrane are within approximately a Debye length. For longer separations, the two converge. For large separations, the energy of membrane-vesicle interaction can be given by Eq. S16, and the force between the vesicle and membrane is given by Eq. S17. Equation S17 shows that there is a very steep dependence of the repulsive electrostatic force on the separation between the vesicles and the membrane (see Fig. S3), and at a 5 nm separation this force becomes negligibly small ($<$1 pN).

Simulations of SNARE unzipping under external forces suggest that membrane-vesicle repulsion is unlikely to separate the bundle beyond layer 7

To understand how the electrostatic repulsion between the vesicle and the membrane would affect SNARE zippering, we performed MD simulations with an external force applied to the C-terminal residue of Syb, W89, and directed perpendicular to the SNARE bundle (Fig. 2 *A*). The C-terminal residue of Syx (K256), C-terminal residue of SN1 (K83), and N-terminal residue of SN2 (G139) had their Cα atoms fixed, to imitate the attachment of these proteins to the plasma membrane. Applying a force of 140 pN (2 kcal/mol/Å), which is in the middle of the estimated range of electrostatic repulsion (90–210 pN, as calculated in the previous section), produced the separation of the terminal residues of Syx and Syb within nanoseconds (Fig. 2, *B* and *C*), and the complex stabilized at a distance of 2–3 nm between Syx and Syb C-terminus residues. The simulations were repeated three times, starting from different points of the SNARE MD trajectory. A detailed examination of the unzipping pathway shows that the complex is stabilized by hydrophobic interactions of L84 of Syb (layer 8), a salt bridge between K85 of Syb and D250 of Syx (layer 7), and hydrophobic

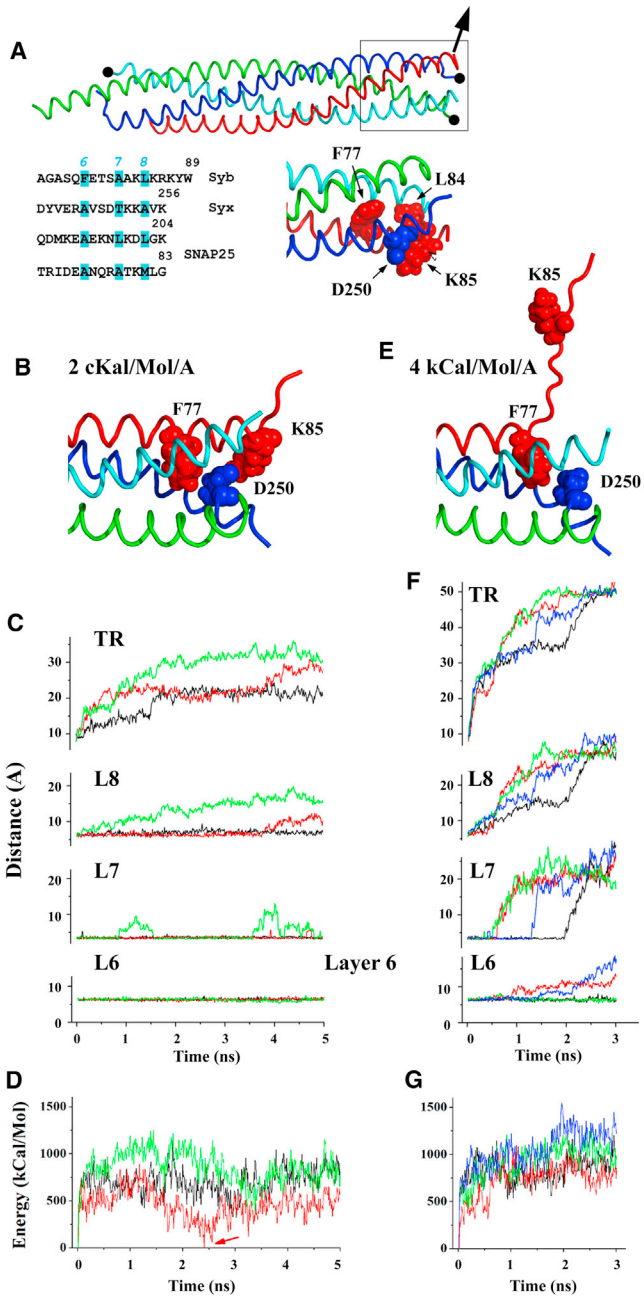

FIGURE 2 Dynamics of SNARE unzipping under external forces. (*A*) Simulation design: the Cα atoms of the Syx C-terminal residue, SN1 C-terminal residue, and SN2 N-terminal residue are fixed to imitate the attachment of the SNARE bundle to the plasma membrane (*black circles*), and an external force (*arrow*) is applied to Syb C-terminal residue W89 to imitate the tension exerted by an attached vesicle. The boxed region, including layers 6–8, is shown below, and stabilizing residues are marked. (*B* and *C*) Application of a force of 2 kcal/mol/Å produces a separation of layer 8, but not layer 6. (*B*) The structure obtained at the end of the trajectory. (*C*) Three pathways starting from different points of the equilibrium MD trajectory of the SNARE complex are marked by different colors (*black*, *red*, and *green*). TR, terminal residues; L8, layer 8; L7, layer 7; L6, layer 6. The separation of layer 8 was measured as the distance between Cα atoms of residues L84 of Syb and A254 of Syx; the separation of layer 7 was measured as the distance between the groups forming a salt bridge at equilibrium (i.e., the Cγ atom of D250 of Syx and N_z of K85 of Syb); and the separation of layer 6 was measured as the distance between Cα atoms of the residues F77 of Syb and A247 of Syx. (*D*) During SNARE separation under the force of 2 kcal/mol, the complex passes an energy barrier within the initial 2–3 ns. This energy barrier may be followed by a local minimum (the pathway marked by *red line*; the local energy minimum is indicated by an *arrow*) where an energy of the SNARE complex approaches the baseline. Three lines correspond to trajectories shown in panel *B*. The baseline for each trajectory corresponds to the energy of its starting point. (*E* and *F*) Application of a force of 4 kcal/mol/Å produces a robust separation of layer 7 and sometimes unzippers layer 6 (trajectories marked by *red* and *blue*). Four pathways starting from different points of the MD trajectory are marked by different colors (*black*, *red*, *green*, and *blue*). The labeling is the same as in panel *C*. (*G*) During SNARE separation under a force of 4 kcal/mol, the energy increases robustly, and the energetic costs corresponding to the separation of layer 6 exceed 500 kcal/mol.

interactions of F77 of Syb (layer 6; Fig. 2 *A*). The simulations described above produced a disruption of the interactions of the layer 8 in two replicas out of three (Fig. 2 *C*, layer 8). However, other interactions, including the salt bridge between K85 of Syb and D250 of Syx, stabilizing layer 7 (Fig. 2, *B* and *C*, layer 7), as well as hydrophobic interactions of F77 of Syb, stabilizing layer 6 (Fig. 2, *B* and *C*, layer 6), remained intact.

To explore the energetic costs of the unzippering pathway presented in Fig. 2, *B* and *C*, we calculated the increase in protein energy along each trajectory (Fig. 2 *D*). The lowest-energy pathway (Fig. 2 *D*, *red line*) corresponded to the trajectory with a very modest separation of layer 8 and with layer 7 intact. Along this trajectory, the complex passed an energy barrier and reached a low-energy state (Fig. 2 *D*, arrow). Hypothetically, such a partially unzipped complex may represent an intermediate metastable state in the sequence of events leading to vesicle fusion. Our computations demonstrate that the electrostatic membrane-vesicle repulsion may be sufficient to generate such a state of the SNARE complex, and that its energetic costs are low.

We questioned whether a more radical unzippering is likely. One could argue that the simulation was performed at the scale of several nanoseconds, and a longer application of constant external forces would produce a more radical separation, as was observed experimentally (42). However, the force produced by the membrane-vesicle electrostatic repulsion is not constant but distance dependent (Fig. S3). Importantly, at the observed separation ($\geq$2 nm; Fig. 2 *B*), the repulsive force would decrease by an order of magnitude (Fig. S3), and hence is unlikely to produce a further separation of the layers. Thus, our simulations predict that the membrane-vesicle repulsion would produce a SNARE equilibrium state with the helical structure of the C-terminus of Syb being disrupted, and possibly the hydrophobic residues of layer 8 being partially separated, but with the other layers intact (Fig. 2 *B*).

To test whether a stronger force could trigger an alternative pathway for SNARE unzipping, and to push the limits, we doubled the external force applied to Syb, taking it outside the range predicted for electrostatic repulsion.

This force (280 pN) produced a faster separation of the bundle (Fig. 2, *E* and *F*), as well as a separation of layer 6 in two replicas out of four. The complex unzippered in a way that is similar to the separation pathway observed at a weaker force: an extension of the Syb C-terminus and melting of its helical structure was followed by a separation of layer 8 residues of Syb and Syx, a separation of layer 8 residues of Syb and SN2, the disruption of the salt bridge between K85 of Syb and D250 of Syx, and in two cases out of four, a separation of layer 6. The energetic costs of such unzippering were very high (Fig. 2 *G*). Importantly, by the time layer 6 unzipping was triggered, Syb and Syx C-termini were separated by $\geq$4 nm, which corresponds to the decrease in repulsive forces by 2 orders of magnitude (Fig. S3). Upon withdrawal of the external force, layer 6 zipped within 5 ns (Fig. S4). This result demonstrates that the electrostatic repulsion between the vesicle and the membrane is unlikely to unzip layer 6.

Thus, our results suggest that the electrostatic repulsion between the vesicle and the membrane is likely to separate the terminal residues of Syb and Syx, and possibly the residues of layer 8, but is unlikely to disrupt layer 6. It should be noted, however, that the simulations described above imitate SNARE separation, whereas exocytosis involves a reverse process, SNARE assembly. To simulate the final stages of this process, we created three different states of the SNARE complex with a partially unzipped C-terminus, including layers 7 and 8, with terminal residues of Syb and Syx separated by 5 nm (Figs. 2 *D* and 3 *A*). We created these initial states by applying a force of 280 pN to the Syb C-terminus, as described above, at different points of the SNARE trajectory. Subsequently, we investigated the relaxation of these partially unzipped SNARE complexes.

One problem with unconstrained simulations of the relaxation process was that the unstructured Syb C-terminus sometimes bent and interacted with a central part of Syb (Fig. S5). Clearly, this does not correspond to a realistic situation in which an attached vesicle would prevent such interactions. To imitate a tension exerted by the attached vesicle to the Syb transmembrane domain, we introduced a weak holding force (0.5 or 1 k_BT/Å) applied to the Syb C-terminal residue. We found that the relaxation kinetics was similar for force values of 0.5 and 1 k_BT/Å (Fig. S5), and therefore we performed all subsequent simulations under a holding force of 0.5 k_BT/Å.

The MD times employed (105–110 ns) were not sufficient to simulate full zippering of the SNARE C-terminus. However, partial zipping was observed in all three trajectories (Fig. S6, *A* and *B*), and the distance between the C-terminal residues of Syx and Syb was reduced to ~3.5 nm within the initial 2–3 ns of the simulation. This was associated with partial zipping of layer 8 (Fig. S6 *C*). Subsequently, the complex progressed through partially zipped states (Fig. S6 *A*). In one of the trajectories (Fig. S6, *B* and *C*, *black*), the salt bridge between K85 of Syb and D250 of Syx, stabilizing layer 7, was formed after 66 ns of the simulation (Fig. S6, *A–C*, state 4); however, this conformation remained stable for only 3 ns. Importantly, high energy levels (Fig. S6 *D*, 500–1200 kcal/mol above the baseline, which corresponded to the energy of a fully zipped SNARE) of the partially unzipped SNARE complex suggest that such a state would not be stable, and further zipping would occur at longer timescales. Thus, stabilization of layer 7 by the formation of a salt bridge between K85 of Syb and D250 of Syx, as observed in equilibrium as well as in state 4 (Fig. S6 *A*), is likely to occur at longer timescales. It should be noted that the holding force employed in our simulations exceeded the electrostatic repulsion calculated for the distance range examined (0.1 k_BT/Å at a distance of 3.5 nm; Fig. 3), and thus electrostatic repulsion would not interfere with further SNARE assembly.

By combining analysis of vesicle-membrane electrostatic interactions with MD simulations of the SNARE complex under external forces, we demonstrated that the electrostatic vesicle-membrane repulsion is likely to produce only very subtle SNARE unzipping (as shown in Fig. 2 *B*), with layer 6 and probably layer 7 playing a critical role in stabilizing the SNARE complex.

Cpx AH stabilizes a partially unzipped SNARE C-terminus

We hypothesized that if the clamped state corresponds to the partially unassembled SNARE complex, Cpx would stabilize such a state as a fusion clamp. To test this hypothesis, we repeated the relaxation simulations in the presence of Cpx (Figs. 3 and S6). First, as described in the previous section, we generated three states of the SNARE/Cpx complex with layers 7 and 8 being separated, and the distance between the terminal residues of Syb and Syx being equal to 5 nm. Interestingly, we found that in all three states the Syb C-terminus was interacting with Cpx (Fig. 3 *A*). Typically, these interactions involved residues K37 and L41 of Cpx. One could expect, therefore, that the van der Waals interactions of the partially unstructured Syb C-terminus with the Cpx AH might increase the rigidity of the entire molecular complex and thus stabilize the partially unzipped state of the SNARE bundle. To test this hypothesis, we performed relaxation simulations of the partially unzipped SNARE/Cpx complex similar to those described in the previous section.

We found that none of the three partially unzipped SNARE states showed a tendency to assemble in the presence of Cpx (Fig. S6, *E–G*). This result suggests that the presence of the Cpx AH could stabilize the SNARE state with unzipped layers 7 and 8, which would produce a separation between the vesicle and membrane at ~5 nm. Indeed, in the presence of Cpx, a more radical separation of the C-terminus layers of the SNARE complex was observed (Fig. 3, *A* and *B*). Importantly, the energy declined

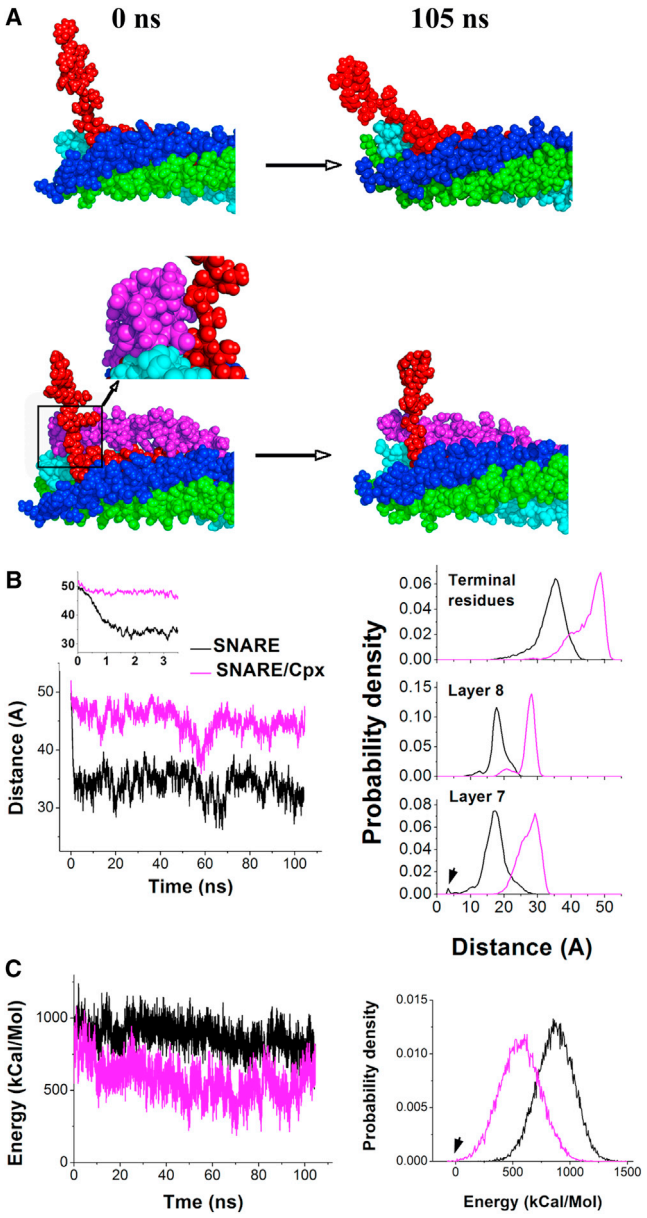

FIGURE 3 Cpx may stabilize a state of the SNARE complex with unzipped layers 7 and 8. (*A*) SNARE complex without (*top*) and with (*bottom*) Cpx with separated layers 7 and 8 at the beginning (*left*) and end (*right*) of a 105 ns MD simulation of the relaxation. Syb (*red*) came into closer contact with the SNARE bundle in the absence of Cpx. The inset shows the enlarged region (*box*), which is also rotated to show the van der Waals interactions of Syb and Cpx. (*B*) The presence of Cpx produces a more radical separation of the C-terminus layers of the SNARE complex over the entire trajectory. The distance between the C-terminal residues (C_α atoms) of Syb and Syx (*left*) decays rapidly in the absence of CPX (*black line*), but not in its presence (*magenta*). The inset shows the decay in distance within the initial 3.5 ns. The lines represent the average of three independent runs (individual runs are shown in Fig. S5). The separation of Syb and Syx C-terminal residues, layer 8, and layer 7 (*right*) is increased in the presence of Cpx (*magenta*). The probability density was calculated at the 5–105 ns time period of the trajectory, so the initial period of fast relaxation of the SNARE complex was excluded from the probability density analysis. The trajectories obtained from three independent runs for each complex were pooled together to calculate probability densities. An arrow (layer 7) indicates the state with a stabilizing salt bridge between D250 of Syx and K85 of Syb being formed. (*C*) The energy of the SNARE/Cpx complex (*magenta*) shows a stronger tendency to decrease and lies below the energy of the SNARE complex (*black*) over the entire trajectory. The time course (*left*) shows the average of three runs, and the probability density (*right*) was calculated over the time period of 5–105 ns by pooling the data from all three trajectories for each complex. The arrow (*right*) indicates the energy overlapping with the baseline (fully zippered bundle at equilibrium) for the SNARE/Cpx complex.

consistently along all three trajectories, and was reduced to 300–700 kcal/mol at the end of the simulations (Figs. 3 *C* and S6 *H*). At the lowest-energy time points (Fig. 3 *C*, *arrow*; Fig. S6 *H*), the energy crossed the baseline. In contrast, in the absence of Cpx, the energy stayed significantly above the baseline over the entire length of the simulation (Figs. 3 *C* and S6 *D*). This result suggests that the presence of Cpx tends to stabilize the partially unzipped state of the SNARE complex with layers 7 and 8 being separated.

Our findings demonstrate that although electrostatic forces are not sufficient to stabilize the partially unzipped SNARE complex with separated layers 7 and 8, such a state is likely be stabilized by the presence of Cpx and its interactions with Syb. These results support a model in which the SNARE bundle with separated layers 7 and 8 may represent the clamped fusion state, and Cpx stabilizes such a clamped state (Fig. 4). This hypothesis is in line with studies demonstrating that mutations that destabilize layers 7 and 8 of the SNARE bundle arrest spontaneous release (20), whereas mutations in layer 6 disrupt the entire fusion process (21).

If this is the case, we would expect a mutant with an unclamping phenotype to have impaired Syb-Cpx interactions. To test this prediction, we took advantage of the $syx^{3\text{-}69}$ TS paralytic *Drosophila* mutant (28), which has enhanced spontaneous release partially mimicking the phenotype of the *cpx* null mutant (29).

The Syx T251I mutation modifies the position of the Cpx AH, stabilizing its interactions with SN2 and diminishing its interactions with Syb

We asked whether our model could explain the *cpx*-like enhanced spontaneous release phenotype in the TS paralytic *Drosophila* mutant $syx^{3\text{-}69}$. This mutation (T354I substitution in *Drosophila* Syx, corresponding to T351I in the mammalian isoform) was discovered in a *Drosophila* screen for TS mutants that disrupt locomotion (28). A subsequent study (29) revealed that the $syx^{3\text{-}69}$ line has a drastically increased frequency of spontaneous release. Besides mutations in *cpx*, this is the only reported *Drosophila* mutant discovered so far that shows a strong *cpx*-like phenotype of enhanced spontaneous fusion. The T251 residue is positioned in layer 7 and its side chain faces inside the SNARE bundle and does not interact directly with Cpx. However, it interacts closely with residue A81 of Syb, which is next to Syb residue K83 (Fig. 5 *A*) that forms a salt bridge with

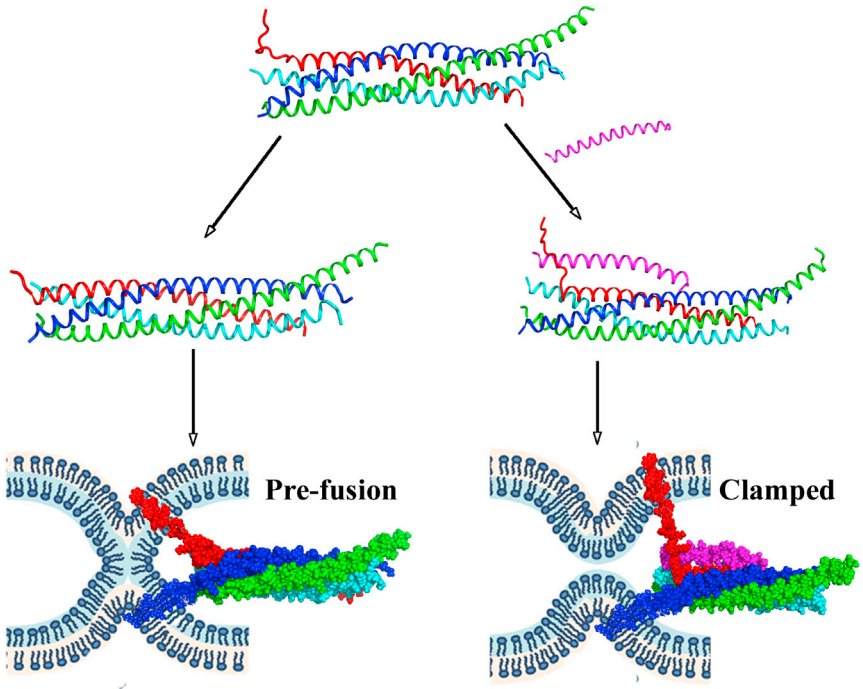

FIGURE 4 Model of the fusion clamp. Cpx (*magenta*) stabilizes the clamped state in which layers 7 and 8 of the SNARE bundle are unzipped, and thus the vesicle and plasma membranes are separated. In the absence of Cpx, Syb comes into closer contact with the rest of the SNARE bundle, which brings the membranes together and creates the stalk, or prefusion state.

E34 of Cpx. As such, disruption of this residue could potentially alter the interactions of Syb residue K83, including its binding to Cpx. Although the mutated residue does not come into direct contact with Cpx, it is positioned such that it could indirectly alter the Cpx bound state. To determine whether the Syx mutant would alter the conformational changes we found for Cpx, we performed MD simulations of the mutated SNARE/Cpx complex.

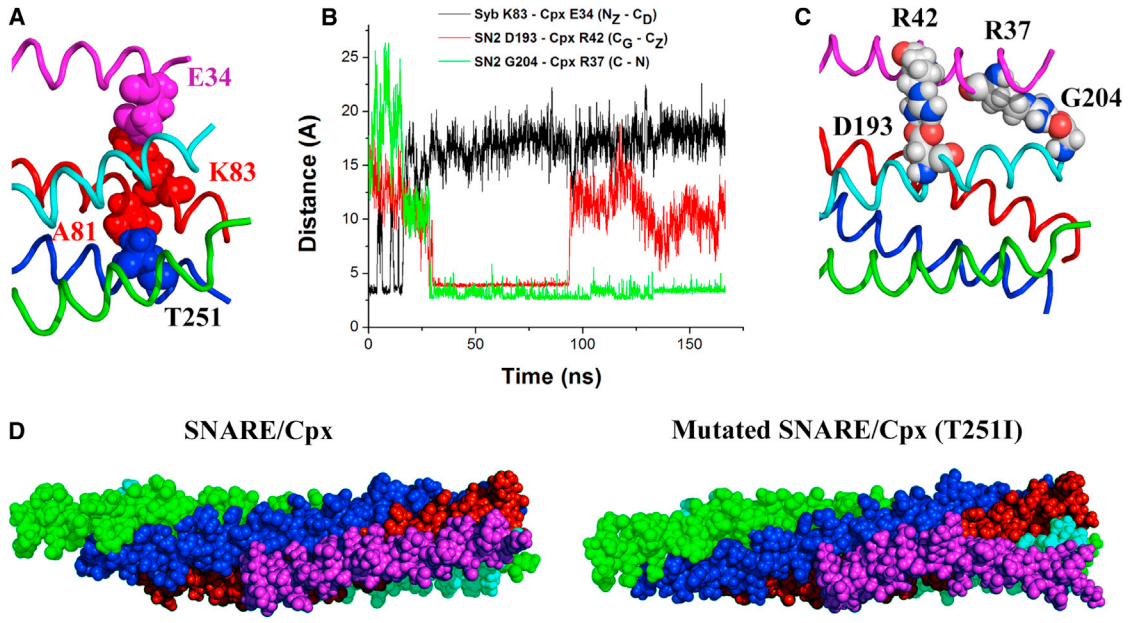

FIGURE 5 The T251I point mutation in syntaxin changes the Cpx conformation. (*A*) The side chain of residue T251 of Syx faces inside of the SNARE bundle and interacts with A81 of Syb, and thus is positioned so that it can potentially alter the interactions of Syb (*red*) and Cpx (*magenta*). (*B* and *C*) MD simulation of the mutated SNARE/Cpx complex shows the disruption of the salt bridge between Syb and Cpx (K83 of Syb–E34 of Cpx) and the formation of two salt bridges between Cpx and SN2 (*C*), one of which (R42 of Cpx–D193 of SN2, *red line*) is subsequently disrupted. (*D*) The mutated SNARE/Cpx complex (*right*) at the end of its MD trajectory (*B*) has a Cpx conformation that differs significantly from that in the nonmutated SNARE/Cpx complex (*left*). In the mutated complex, Cpx (*magenta*) deviates from Syb (*red*).

As a starting point for the MD simulations, we took the MC-optimized conformation of the SNARE/Cpx complex in a water-ion environment and introduced the T251I point mutation. Subsequently, we performed a 165 ns MD simulation. Notably, we found that the Syx T251I mutation radically changed the trajectory of the SNARE/Cpx complex and the equilibrium position of the Cpx AH (Fig. 5, *B–D*). After 25 ns of the simulation, the Cpx AH formed close contacts with SN2, but not with Syb. The salt bridge supporting the Syb-Cpx interactions was disrupted within the initial 20 ns of the MD trajectory (Fig. 5 *B*, *black line*). Similar to what was observed for the nonmutated SNARE/Cpx complex, Cpx-SN2 interactions were stabilized by a salt bridge between R42 of Cpx and D193 of SN2 (Fig. 5 *B*, *red line*, and *C*). In addition, an even more stable salt bridge was formed between R37 of Cpx and G204 of SN2 (Fig. 5 *B*, *green line*, and *C*). The overall position of Cpx was changed in the mutated complex: the Cpx AH deviated from lying almost parallel to Syb, and a kink appeared between the Cpx CH and AH to accommodate the interactions of the Cpx AH with the SN2 C-terminus (Fig. 5 *D*).

These MD simulations demonstrate that the position of the Cpx AH is modified in the $syx^{3\text{-}69}$ mutant, and interactions of the Cpx AH with Syb are disrupted. These data suggest that Syb would be less likely to come into a contact with the Cpx AH during SNARE assembly. Since our model (Fig. 4) proposes that the Cpx clamping function critically depends on the interactions of the Cpx AH with Syb during the final steps of SNARE assembly, we would predict that the clamping function in the $syx^{3\text{-}69}$ mutant would be weakened.

To enable a direct quantitative comparison of transmitter release in the $syx^{3\text{-}69}$ mutant with *cpx* null mutants, we performed focal recordings from visualized synaptic boutons at *Drosophila* NMJs (Fig. 6 *A*). Because this technique allows recordings to be obtained from a limited number of active zones, it allows accurate quantification of spontaneous activity even if it is drastically elevated, as is the case with *cpx*. We found that spontaneous release was enhanced in the $syx^{3\text{-}69}$ mutant; however, it was less severe than that observed in *cpx* null mutants (Fig. 6, *B* and *C*). Our findings in vivo are consistent with the partial loss of function of the Cpx AH, which undergoes a conformational shift due to the mutation in Syx.

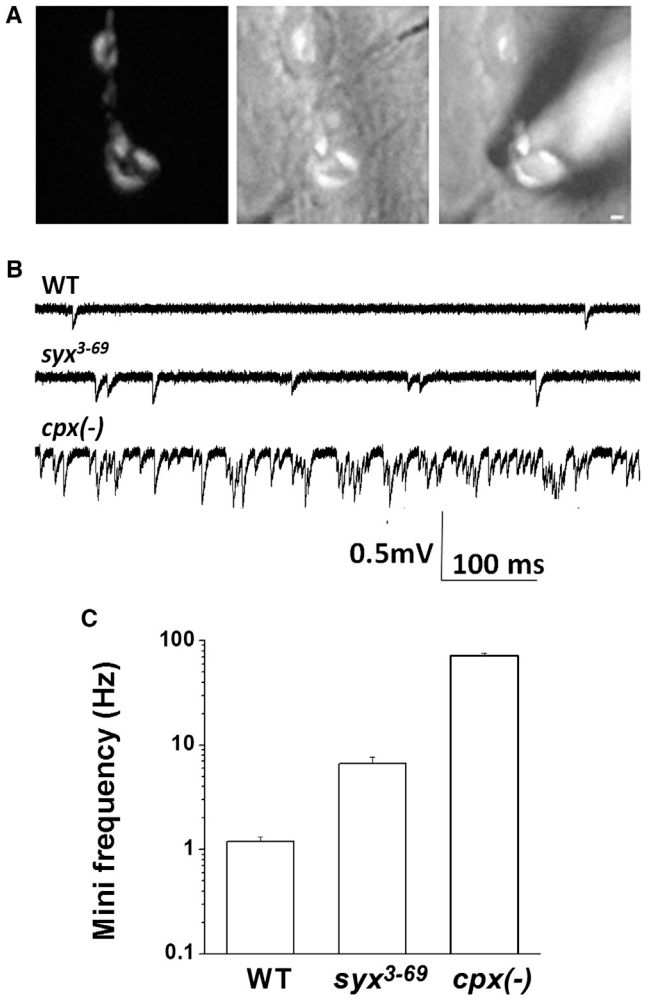

FIGURE 6 Spontaneous release is unclamped in $syx^{3\text{-}69}$ and cpx^{SH1} null *Drosophila* mutants. (*A*) Focal recordings of spontaneous activity from visualized boutons. Left: FM1-43 staining; middle: overlay with the bright-field image; right: overlay with the recording electrode. (*B*) Representative recordings of spontaneous activity. (*C*) The frequency of miniature synaptic responses is moderately enhanced in the $syx^{3\text{-}69}$ mutant and strongly enhanced in the *cpx* null mutant. Error bars denote SE.

DISCUSSION

In this work, we performed a computational analysis of the three-dimensional structure of the SNARE complex to understand the mechanism of fusion clamping. We found that in a water-ion environment, the Cpx AH forms a tight complex with the SNARE bundle, in contrast to the Cpx AH conformation observed by crystallography (18). To explore the hypothesis that the SNARE clamped state corresponds to the partially unzipped SNARE C-terminus, we calculated electrostatic repulsion between the vesicle and the membrane, and performed MD simulations of the SNARE complex under external forces. We demonstrated that the membrane-vesicle repulsion is likely to unzip layer 8 of the SNARE bundle, but is unlikely to produce a more radical separation because the highly hydrophobic residues of layer 6 work as a zipper. Importantly, we found that Cpx binding stabilizes a partially unzipped conformation of the Syb C-terminus, with separated layers 7 and 8. Such a partially unzipped SNARE state would create an efficient clamp in merging the two membranes (Fig. 4).

Electrostatic repulsion between the vesicle and the membrane versus SNARE zippering

SNARE complex assembly proceeds rapidly from the N- to C-terminus (43). It has been proposed that the degree of

SNARE complex assembly may determine the readiness of a vesicle for the release process (44), and that a partially assembled SNARE complex may correspond to the primed vesicle state (21,45). Consistent with this model, a fusion clamping mechanism was been proposed (5,6) whereby Cpx arrests the SNARE complex in a partially unzipped state, with layers 2–8 of Syb being separated from the SNARE bundle. On the other hand, an alternative view was proposed (23) that places the vesicle priming machinery upstream of SNARE nucleation, and suggests that SNAREs act as a single-shot device that, once triggered, would flash through assembly and bring about fusion. The latter scenario is based on the assumption that SNARE pin assembly, at every stage, is a process with high energetic gain, and thus a partially zippered state would not be stabilized. To test this suggestion and to explore the two competitive scenarios outlined above, we simulated the processes of assembly/disassembly of the SNARE C-terminus.

Combining calculations of the vesicle-membrane electrostatic interactions with MD simulations of the SNARE complex under external forces, we found that the electrostatic repulsion between the membrane and the vesicle is not strong enough to produce a radical unzipping of the SNARE complex. Our computations demonstrate that unzipping the C-terminal layers 7 and 8 of the SNARE bundle would separate the vesicle and the membrane by ~5 nm, and at such a distance the membrane-vesicle repulsion would be negligibly small and thus would not prevent SNARE assembly.

However, the electrostatic repulsion increases drastically as the distance between the membrane and the vesicle diminishes. We demonstrated that at a distance of 1 nm, this repulsion is strong enough to trigger separation of layer 8 of Syb from t-SNARE. This result argues that SNARE assembly is unlikely to function as a single-shot device, and that the complex with an unzipped layer 8 is likely to stabilize due to electrostatic forces. At such a state of the SNARE bundle, the vesicle and membrane would be separated by 2–3 nm, a distance comparable to the size of a synaptotagmin molecule. Thus, electrostatic repulsion between the membrane and the vesicle is likely to maintain the SNARE complex in a state that is close to being fully zippered, and in which the membranes are close enough to be brought into contact by Ca^{2+}-sensing proteins that can trigger fusion, such as synaptotagmin.

It is of interest to compare the SNARE unzippering pathway suggested by our simulations with the results of a recent single-molecule study that examined SNARE separation with the use of optical tweezers (42). The latter study revealed four stages of SNARE disassembly, including three-stage unzipping of the C-terminus domain, characterized by extensions of 3, 7, and 15 nm, and a radical unfolding of the N-terminal domain. In our simulations, we observed the disassembly of SNARE layers 7 and 8, which is characterized by 3–5 nm extensions and is likely to represent the first disassembly stage. We found that highly hydrophobic interactions of layer 6 stabilize this stage. Notably, the forces required to transition to the next disassembly stage (14–19 pN (42)) exceed the electrostatic repulsion forces (<5 pN, as predicted by our computations) that would be exerted by the vesicle and the membrane at this stage of disassembly.

The Cpx AH forms tight links with the SNARE bundle at equilibrium and may stabilize a partially unzipped state of synaptobrevin

The Cpx AH was shown to play a critical role in the Cpx clamping function (10). However, the x-ray analysis demonstrated that the Cpx AH does not interact with the SNARE bundle (18). We performed prolonged MD simulations of the SNARE/Cpx complex in the water-ion environment and found that under these conditions, Cpx forms tighter links with the SNARE bundle compared with those observed by crystallography. Importantly, the Cpx AH comes into tight contact with both Syb and SN2, and stabilizing salt bridges are formed between Cpx and both proteins. These tight interactions between the Cpx AH and the SNARE C-terminus could explain the influence of the Cpx AH on assembly and disassembly of the SNARE C-terminus.

In support of this model, we found that the Cpx AH interacts with Syb even when the SNARE C-terminus is partially unzipped. Furthermore, we found that the Cpx AH, interacting with Syb, stabilizes this partially unzipped state. This finding supports a model in which the clamped state of the release-ready synaptic vesicle would correspond to the SNARE bundle with separated layers 7 and 8, stabilized by interactions with Cpx (Fig. 5). Such a fusion clamp would maintain the vesicle at a distance of ~5 nm, out of the range for synaptotagmin to bring the membranes together and trigger fusion (46). In the absence of Cpx, such a state would not be stable, SNARE assembly would proceed, and the membranes would be brought to a closer distance (2–3 nm), where membrane fusion could be triggered.

Two molecular models of the Cpx fusion clamp have been previously suggested. The first model (5) proposed that the clamped state corresponds to a partially unzipped C-terminus of Syb, which is displaced by the Cpx AH. A subsequent model (6) refined this view, proposing that several SNARE complexes form a highly organized pattern cross-linked by Cpx molecules to clamp the fusion. Both models share two critical common features: 1), the clamped state of the SNARE complex corresponds to a partially unzipped SNARE C-terminus; and 2), Cpx promotes the clamped state by displacing the Syb C-terminus from the SNARE bundle.

Our model agrees with this view in suggesting that the clamped state corresponds to the partially unzipped SNARE C-terminus, and that Cpx is able to promote this state.

However, we propose an alternative mechanism for this Cpx action, which is more parsimonious energetically. Our model suggests a subtle unzipping of the SNARE C-terminus, which has lower energetic costs. Extensive unzipping was necessary for earlier models to allow for a topology in which Cpx can replace Syb. Thus, both of the earlier models (5,6) proposed that Syb separates from the SNARE bundle through residue 60, which includes layers 2–8 of the SNARE bundle. However, our computations suggest that the separation of layer 6 of the SNARE bundle is likely to require forces exceeding those produced by the membrane-vesicle electrostatic repulsion. This view is supported by the finding that the highly hydrophobic Syb residue F77, belonging to layer 6 of the SNARE bundle, is critical for exocytosis (21). Importantly, our model does not require a conformational state of the SNARE complex with the radically unzippered C-terminus. We demonstrate that Cpx may stabilize a partially disassembled SNARE bundle without displacing Syb.

Importantly, our model has the capability to derive specific predictions for targeted mutagenesis, and this approach enables us to test its predictive power. Our model predicts that the interactions between Syb and Cpx, such as the salt bridge between E34 of Cpx and K83 of Syb, are critical for fusion clamping, and that disrupting these interactions by mutating either residue would alter the Cpx clamping function. Further experimentation is needed to test this prediction. In this study, we took advantage of an existing syntaxin mutant with abnormal spontaneous release and tested whether our model is capable of explaining its phenotype.

The T251I mutation in syntaxin displaces the Cpx AH, which may explain the enhanced spontaneous fusion in the $syx^{3\text{-}69}$ Drosophila mutant

We tested whether our model could explain the increased spontaneous activity in the TS paralytic mutant $syx^{3\text{-}69}$ (28,29), which to date is the only *Drosophila* mutant known to demonstrate an increase in spontaneous fusion rates comparable to that observed for the *cpx* null phenotype. It should be noted, however, that our direct comparison of spontaneous activity in $syx^{3\text{-}69}$ and *cpx* lines (performed here with a recording technique that enables careful quantification) demonstrated a severalfold lower spontaneous activity in $syx^{3\text{-}69}$ compared with *cpx*, although it was still drastically increased compared with controls.

When we examined the Syx point mutation present in $syx^{3\text{-}69}$, the substitution of Thr-254 by Ile in Syx (corresponding to T251I in mammalian syntaxin), we found that this mutation could alter the dynamics of the SNARE C-terminus layers 7 and 8, since residue T251 belongs to layer 7 and its side chain faces inside the bundle. However, without thorough MD computations, it would be almost impossible to predict how specifically these dynamics would be affected. It should be noted that the T251I point mutation was examined with the use of MD computations in an earlier study (29), and no effect of this mutation on the SNARE C-terminus dynamics was reported. However, that study did not consider how this mutation could affect the dynamics of Cpx. Employing MD of the mutated SNARE/Cpx complex, we found that the mutation affects binding of the Cpx AH to layers 7 and 8 of the SNARE bundle, and that it promotes the state of Cpx in which its AH is detached from Syb. Because our model predicts that interactions of the Cpx AH with Syb are critical for clamping, the latter finding drives the prediction that the T254I mutation in *Drosophila* would produce a phenotype that would partially mimic Cpx deficiency, which is what we observe experimentally.

SUPPORTING MATERIAL

One table, six figures, and seventeen equations are available at http://www.biophysj.org/biophysj/supplemental/S0006-3495(13)00697-8.

We thank Dr. Boris Zhorov for kindly providing us with ZMM software and for helpful discussions.

This study was supported by grants U54 NS039408 and R01 MH099557 from the National Institutes of Health. For MD computations, we used the Extreme Science and Engineering Discovery Environment, which is supported by National Science Foundation grant number OCI-1053575, and specifically the Texas Advanced Computing Center under grant number TG-MCB100049 and the National Institute of Computational Science. The VMD/NAMD software was developed by the Theoretical and Computational Biophysics group at the Beckman Institute, University of Illinois at Urbana-Champaign, with support from the National Institutes of Health.

REFERENCES

1. Huntwork, S., and J. T. Littleton. 2007. A complexin fusion clamp regulates spontaneous neurotransmitter release and synaptic growth. *Nat. Neurosci.* 10:1235–1237.
2. Jorquera, R. A., S. Huntwork-Rodriguez, …, J. T. Littleton. 2012. Complexin controls spontaneous and evoked neurotransmitter release by regulating the timing and properties of synaptotagmin activity. *J. Neurosci.* 32:18234–18245.
3. Maximov, A., J. Tang, …, T. C. Südhof. 2009. Complexin controls the force transfer from SNARE complexes to membranes in fusion. *Science.* 323:516–521.
4. Cho, R. W., Y. Song, and J. T. Littleton. 2010. Comparative analysis of Drosophila and mammalian complexins as fusion clamps and facilitators of neurotransmitter release. *Mol. Cell. Neurosci.* 45:389–397.
5. Giraudo, C. G., A. Garcia-Diaz, …, J. E. Rothman. 2009. Alternative zippering as an on-off switch for SNARE-mediated fusion. *Science.* 323:512–516.
6. Kümmel, D., S. S. Krishnakumar, …, K. M. Reinisch. 2011. Complexin cross-links prefusion SNAREs into a zigzag array. *Nat. Struct. Mol. Biol.* 18:927–933.
7. Hobson, R. J., Q. Liu, …, E. M. Jorgensen. 2011. Complexin maintains vesicles in the primed state in C. elegans. *Curr. Biol.* 21:106–113.
8. Martin, J. A., Z. Hu, …, J. S. Dittman. 2011. Complexin has opposite effects on two modes of synaptic vesicle fusion. *Curr. Biol.* 21:97–105.
9. Reim, K., M. Mansour, …, C. Rosenmund. 2001. Complexins regulate a late step in Ca^{2+}-dependent neurotransmitter release. *Cell.* 104:71–81.

10. Xue, M., K. Reim, …, C. Rosenmund. 2007. Distinct domains of complexin I differentially regulate neurotransmitter release. *Nat. Struct. Mol. Biol.* 14:949–958.

11. Lai, Y., J. Diao, …, Y. K. Shin. 2013. Fusion pore formation and expansion induced by Ca2+ and synaptotagmin 1. *Proc. Natl. Acad. Sci. USA.* 110:1333–1338.

12. Giraudo, C. G., W. S. Eng, …, J. E. Rothman. 2006. A clamping mechanism involved in SNARE-dependent exocytosis. *Science.* 313:676–680.

13. Schaub, J. R., X. B. Lu, …, J. A. McNew. 2006. Hemifusion arrest by complexin is relieved by Ca2+-synaptotagmin I. *Nat. Struct. Mol. Biol.* 13:748–750.

14. Reim, K., H. Wegmeyer, …, N. Brose. 2005. Structurally and functionally unique complexins at retinal ribbon synapses. *J. Cell Biol.* 169:669–680.

15. Xue, M., A. Stradomska, …, K. Reim. 2008. Complexins facilitate neurotransmitter release at excitatory and inhibitory synapses in mammalian central nervous system. *Proc. Natl. Acad. Sci. USA.* 105:7875–7880.

16. Strenzke, N., S. Chanda, …, T. Moser. 2009. Complexin-I is required for high-fidelity transmission at the endbulb of Held auditory synapse. *J. Neurosci.* 29:7991–8004.

17. Xue, M. S., T. K. Craig, …, C. Rosenmund. 2010. Binding of the complexin N terminus to the SNARE complex potentiates synaptic-vesicle fusogenicity. *Nat. Struct. Mol. Biol.* 17:568–575.

18. Chen, X. C., D. R. Tomchick, …, J. Rizo. 2002. Three-dimensional structure of the complexin/SNARE complex. *Neuron.* 33:397–409.

19. Yang, X. F., Y. J. Kaeser-Woo, …, T. C. Südhof. 2010. Complexin clamps asynchronous release by blocking a secondary Ca(2+) sensor via its accessory α helix. *Neuron.* 68:907–920.

20. Weber, J. P., K. Reim, and J. B. Sørensen. 2010. Opposing functions of two sub-domains of the SNARE-complex in neurotransmission. *EMBO J.* 29:2477–2490.

21. Walter, A. M., K. Wiederhold, …, J. B. Sørensen. 2010. Synaptobrevin N-terminally bound to syntaxin-SNAP-25 defines the primed vesicle state in regulated exocytosis. *J. Cell Biol.* 188:401–413.

22. Lu, B., S. Song, and Y. K. Shin. 2010. Accessory α-helix of complexin I can displace VAMP2 locally in the complexin-SNARE quaternary complex. *J. Mol. Biol.* 396:602–609.

23. Jahn, R., and D. Fasshauer. 2012. Molecular machines governing exocytosis of synaptic vesicles. *Nature.* 490:201–207.

24. Durrieu, M. P., R. Lavery, and M. Baaden. 2008. Interactions between neuronal fusion proteins explored by molecular dynamics. *Biophys. J.* 94:3436–3446.

25. Durrieu, M. P., P. J. Bond, …, M. Baaden. 2009. Coarse-grain simulations of the R-SNARE fusion protein in its membrane environment detect long-lived conformational sub-states. *ChemPhysChem.* 10:1548–1552.

26. Bock, L. V., B. Hutchings, …, D. J. Woodbury. 2010. Chemomechanical regulation of SNARE proteins studied with molecular dynamics simulations. *Biophys. J.* 99:1221–1230.

27. Ghahremanpour, M. M., F. Mehrnejad, and M. E. Moghaddam. 2010. Structural studies of SNARE complex and its interaction with complexin by molecular dynamics simulation. *Biopolymers.* 93:560–570.

28. Littleton, J. T., E. R. Chapman, …, B. Ganetzky. 1998. Temperature-sensitive paralytic mutations demonstrate that synaptic exocytosis requires SNARE complex assembly and disassembly. *Neuron.* 21:401–413.

29. Lagow, R. D., H. Bao, …, B. Zhang. 2007. Modification of a hydrophobic layer by a point mutation in syntaxin 1A regulates the rate of synaptic vesicle fusion. *PLoS Biol.* 5:e72.

30. Ernst, J. A., and A. T. Brunger. 2003. High resolution structure, stability, and synaptotagmin binding of a truncated neuronal SNARE complex. *J. Biol. Chem.* 278:8630–8636.

31. Li, Z. Q., and H. A. Scheraga. 1987. Monte Carlo-minimization approach to the multiple-minima problem in protein folding. *Proc. Natl. Acad. Sci. USA.* 84:6611–6615.

32. Bruhova, I., and B. S. Zhorov. 2010. A homology model of the pore domain of a voltage-gated calcium channel is consistent with available SCAM data. *J. Gen. Physiol.* 135:261–274.

33. Phillips, J. C., R. Braun, …, K. Schulten. 2005. Scalable molecular dynamics with NAMD. *J. Comput. Chem.* 26:1781–1802.

34. Mackerell, Jr., A. D. 2004. Empirical force fields for biological macromolecules: overview and issues. *J. Comput. Chem.* 25:1584–1604.

35. Lnenicka, G. A., and H. Keshishian. 2000. Identified motor terminals in Drosophila larvae show distinct differences in morphology and physiology. *J. Neurobiol.* 43:186–197.

36. Stewart, B. A., H. L. Atwood, …, C. F. Wu. 1994. Improved stability of Drosophila larval neuromuscular preparations in hemolymph-like physiological solutions. *J. Comp. Physiol. A Neuroethol. Sens. Neural Behav. Physiol.* 175:179–191.

37. Akbergenova, Y., and M. Bykhovskaia. 2007. Synapsin maintains the reserve vesicle pool and spatial segregation of the recycling pool in Drosophila presynaptic boutons. *Brain Res.* 1178:52–64.

38. Akbergenova, Y., and M. Bykhovskaia. 2009. Stimulation-induced formation of the reserve pool of vesicles in Drosophila motor boutons. *J. Neurophysiol.* 101:2423–2433.

39. Bykhovskaia, M. 2008. Making quantal analysis more convenient, fast, and accurate: user-friendly software QUANTAN. *J. Neurosci. Methods.* 168:500–513.

40. Russel, W. B., D. A. Saville, and W. R. Schowalter. 1979. Colloidal Dispersions. Cambridge University Press, New York.

41. Bai, Y., C. R. Jin, …, C. Y. Hui. 2011. Adhesion selectivity by electrostatic complementarity. I. One-dimensional stripes of charge. *J. Appl. Phys.* 110:54902.

42. Gao, Y., S. Zorman, …, Y. L. Zhang. 2012. Single reconstituted neuronal SNARE complexes zipper in three distinct stages. *Science.* 337:1340–1343.

43. Pobbati, A. V., A. Stein, and D. Fasshauer. 2006. N- to C-terminal SNARE complex assembly promotes rapid membrane fusion. *Science.* 313:673–676.

44. Sørensen, J. B., K. Wiederhold, …, D. Fasshauer. 2006. Sequential N- to C-terminal SNARE complex assembly drives priming and fusion of secretory vesicles. *EMBO J.* 25:955–966.

45. Rettig, J., and E. Neher. 2002. Emerging roles of presynaptic proteins in Ca^{++}-triggered exocytosis. *Science.* 298:781–785.

46. Hui, E. F., J. D. Gaffaney, …, E. R. Chapman. 2011. Mechanism and function of synaptotagmin-mediated membrane apposition. *Nat. Struct. Mol. Biol.* 18:813–821.

Interaction of the Complexin Accessory Helix with the C-Terminus of the SNARE Complex: Molecular-Dynamics Model of the Fusion Clamp

Maria Bykhovskaia,[†]* Anand Jagota,[‡§] Agustin Gonzalez,[†] Alexander Vasin,[†] and J. Troy Littleton[¶‖††]

[†]Neuroscience Department, Universidad Central del Caribe, Bayamon, Puerto Rico; [‡]Department of Chemical Engineering and [§]Bioengineering Program, Lehigh University, Bethlehem, Pennsylvania; and [¶]Picower Institute for Learning and Memory, [‖]Department of Biology, and [††]Department of Brain and Cognitive Sciences, Massachusetts Institute of Technology, Cambridge, Massachusetts

Supporting Material

1. Estimate of Electrostatic Force of Repulsion Between a Synaptic Vesicle and a Plasma Membrane

To calculate this force, we considered two polarized planes (the vesicle and the membrane) carrying different surface potentials and separated by a distance (*a).* We modeled the electrostatic potential (φ) along the coordinate (x) which connects the vesicle and the membrane, which can range between 0 and *a*. The electrostatic potential was calculated using the Debye-Huckel equation, which is a linearized version of the nonlinear Poisson-Boltzmann equation [40, 41]:

$$\frac{d^2\varphi}{dx^2} = \frac{\varphi}{l_D^2} \qquad (1)$$

where l_D is the Debye screening length:

$$l_D = \sqrt{\frac{\epsilon\epsilon_0 k_B T}{2q^2 z^2 c_0}},$$

ϵ is the dielectric constant of water, ϵ_0 is the permittivity of free space, q is the charge of an electron, z is the unsigned valence of each of the two ions, c_o is the concentration of the ions, T is temperature, and k_B is Boltzmann's constant. The solution of the equation (1) is:

$$\varphi(\mathrm{x}) = A\cosh\left(\frac{\mathrm{x}}{\mathrm{l_D}}\right) + B\sinh\left(\frac{\mathrm{x}}{\mathrm{l_D}}\right) \qquad (2)$$

To calculate the electrostatic force between the vesicle and the membrane based on Eq. (2), we need to make an assumption about the relationship between the surface potential and surface charge. We have considered two limiting cases:

i. *Surface potential is fixed* and surface charge adjusts to keep it at a constant level. The surface charge could adjust to compensate for the potential change either via redistribution of ions, such as K^+, in the vicinity of the membrane, or via polar lipid groups adjusting their degree of ionization. Both mechanisms would work to minimize the change in the surface potential.

ii. *Surface charge is fixed* and surface potential adjusts. This is the limiting case corresponding to fully ionized groups with a fixed charge.

<u>Fixed Potential</u>

In this case the equation [1] is subject to boundary conditions

a. $\varphi = \varphi_1$ ($x=0$),

b. $\varphi = \varphi_2$ ($x=a$). (3)

where (*x=0*) corresponds to surface '1' and (*x=a*) corresponds to surface '2'. Surface potential on both the vesicle and plasma membrane surface are negative and, without loss of generality, we let $\varphi_2 < \varphi_1$ so that '2' corresponds to the plasma membrane (see Table 1).

Applying the boundary conditions, we find

$$A = \varphi_1$$
$$B = \left[\varphi_2 - \varphi_1 \cosh\left(\frac{a}{l_D}\right)\right] / \sinh\left(\frac{a}{l_D}\right)$$

So that

$$\varphi(x) = \varphi_1 \cosh\left(\frac{x}{l_D}\right) + \left[\varphi_2 - \varphi_1 \cosh\left(\frac{a}{l_D}\right)\right] \sinh\left(\frac{x}{l_D}\right) / \sinh\left(\frac{a}{l_D}\right) \qquad (4)$$

Table 1. Parameters used for calculations of the electrostatic repulsion

	Parameter	Value	Reference	Comment
1	Surface Potential of Vesicle, φ_1	-25 mV	[3]	
2	Surface Potential of Membrane φ_2	-70 mV	[4]	
3	Permittivity ε_o	8.85 x 10^{-12} F/m		SI units
4	Dielectric constant of water ε	80		Dimensionless
5	Salt concentration	200 mM	(1-1 Electrolyte)	
6	Debye Screening Length, l_D	0.67 nm	[5]	$l_D = \sqrt{\frac{\epsilon\epsilon_0 k_B T}{2q^2 z^2 c_0}}$
7	Surface Charge of Vesicle σ_1	-0.0125 C/m^2	[3]	
8	Surface Charge of Vesicle σ_1, σ_2 estimated using assumed surface potential, φ_1	-0.025, -0.07 C/m^2	[3]	$\sigma_1 = \frac{\epsilon\epsilon_0\varphi_1}{l_D}$
9	Separation between vesicle and plasma membrane when SNAREs hold them together	1 nm		
10	Vesicle diameter	45 nm	[3]	

Given the potential, we calculate the force per unit area between the two flat planes using the result [1]

$$f = -\frac{\epsilon\epsilon_0}{2}\left(\frac{d\varphi}{dx}\right)^2 + \frac{\epsilon\epsilon_0}{2}\frac{\varphi^2}{l_D^2} \qquad (5)$$

which yields,

$$f = \frac{\epsilon\epsilon_0}{2l_D^2 \sinh^2(\frac{a}{l_D})}\left(2\varphi_1\varphi_2 \cosh\left(\frac{a}{l_D}\right) - \varphi_1^2 - \varphi_2^2\right) \quad (6)$$

The interaction energy between the two planes is calculated as

$$E \equiv -\frac{Work}{Area} = -\int_{\infty}^{a} f da' \quad (7)$$

which gives

$$E = \frac{\epsilon\epsilon_0}{2l_D}\left(2\varphi_1\varphi_2 \,/\sinh\left(\frac{a}{l_D}\right) - (\varphi_1^2 + \varphi_2^2)(\coth\left(\frac{a}{l_D}\right) - 1)\right) \quad (8)$$

Figure S1 plots the normalized interaction energy, $\frac{2l_D E}{\epsilon\epsilon_0 \varphi_1^2}$ as a function of a/l_D for different values of φ_2/φ_1.

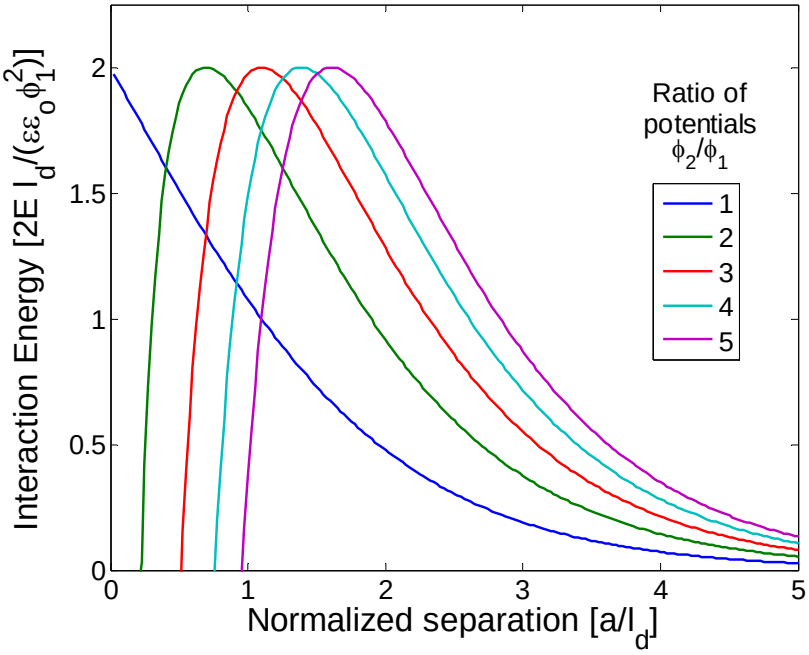

Figure S1. Interaction energy between two planes of charge as a function of ratio of potentials.

This shows some interesting peculiarities. Firstly, even for the same surface potential on both sides, the interaction energy (repulsive) remains bounded even for zero separation. This is because the surface charge reduces in magnitude to keep the surface potential fixed. In fact, at zero separation the surface charge density goes to zero just as the repulsion (for fixed charge) would be going to infinity and the two effects cancel out leaving a finite force. Secondly, for unequal surface potential, there is a maximum in the interaction energy *and this maximum is independent of the larger surface potential.* It depends only on the value of the smaller surface potential. It is given by a very simple expression (energy per unit area)

$$\mathrm{E_{max}} = \frac{\varphi_1^2 \epsilon\epsilon_0}{\mathrm{l_D}} \tag{9}$$

This is the interaction energy between two flat planes. We use Derjaguin's approximation [2], which relates the energy between two flat planes to the force of interaction between a spherical surface and a plane, which is what we need:

$$\mathrm{F_{max}} = 2\pi \mathrm{R_v E_{max}} = 2\pi \mathrm{R_v} \frac{\varphi_1^2 \epsilon\epsilon_0}{\mathrm{l_D}} \tag{10}$$

Fixed Charge

Let us now consider the case where surface charge is held fixed. In this case, the boundary conditions are:

$$-\epsilon\epsilon_0 \frac{d\varphi}{dx} = \sigma_1 \quad (x=0); \;\; \epsilon\epsilon_0 \frac{d\varphi}{dx} = \sigma_2 \;\; (x=a). \tag{11}$$

Applying the boundary conditions, we obtain[1]

$$\varphi(x) = \frac{[\sigma_1 \cosh\left(\frac{a}{l_D}\right) + \sigma_2] l_D}{\epsilon\epsilon_0} \frac{\cosh(\frac{x}{l_D})}{\sinh(\frac{a}{l_D})} - \frac{\sigma_1 l_D}{\epsilon\epsilon_0} \sinh(\frac{x}{l_D}) \tag{12}$$

where σ_1 and σ_2 are the surface charge densities on the two surfaces. The force per unit area is again calculated using equation (6), which gives us

$$f = \frac{\sigma_1^2 + \sigma_2^2 + 2\sigma_1\sigma_2 \cosh\left(\frac{a}{l_D}\right)}{2\epsilon\epsilon_0 \sinh^2(\frac{a}{l_D})} \tag{13}$$

The interaction energy is again calculated using equation (7) and gives us

$$E = \frac{l_D}{2\epsilon\epsilon_0} \left(2\sigma_1\sigma_2 / \sinh\left(\frac{a}{l_D}\right) + (\sigma_1^2 + \sigma_2^2)(\coth\left(\frac{a}{l_D}\right) - 1) \right) \tag{14}$$

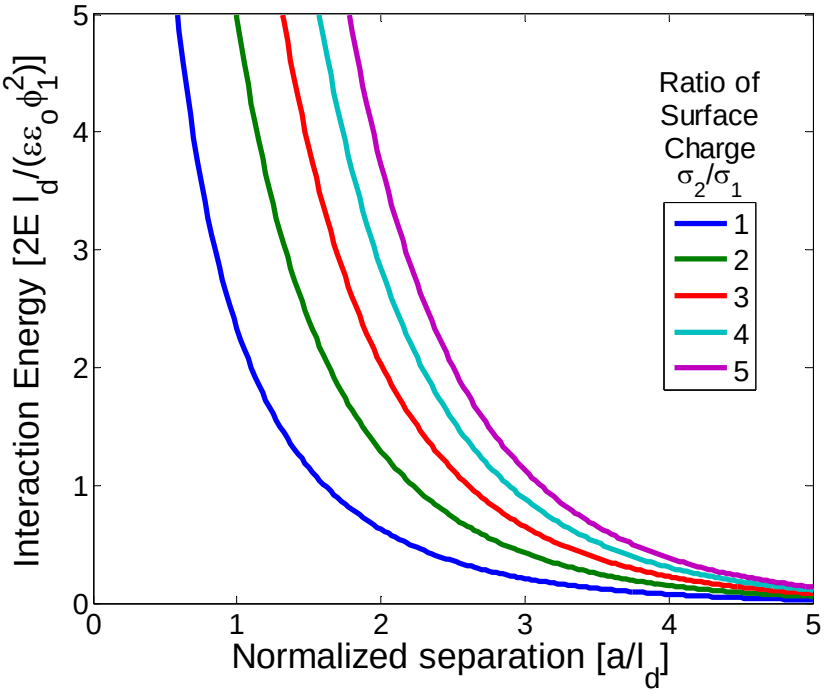

Figure S2 Interaction energy between two charged planes as a function of the ratio of surface charges

Replacing surface charge densities in equation (14) by surface potential at infinite separation, Figure S2 plots the normalized interaction energy, $\frac{2l_D E}{\epsilon\epsilon_0 \varphi_1^2}$ as a function of a/l_D for different values of φ_2/φ_1, w. Now we find that there is always repulsion and it diverges as the two surfaces are brought together. The force is again given by equation (10), i.e.,

$$F = 2\pi R_v E = \frac{\pi R_v l_D}{\epsilon\epsilon_0}\left(2\sigma_1\sigma_2 / \sinh\left(\frac{a}{l_D}\right) + (\sigma_1^2 + \sigma_2^2)(\coth\left(\frac{a}{l_D}\right) - 1)\right) \qquad (15)$$

To estimate the force, we assume a separation of about 1 nm and use other parameters given in Table 1.

Notably, the difference between the fixed potential and fixed charge calculations is significant only when the vesicle and membrane are within about a Debye length. For longer separations, the two converge. In fact, equations (8) and (14) for the energy of interaction both converge to a much simpler formula for large separations:

$$E = \frac{2\epsilon\epsilon_0}{l_D}\varphi_1\varphi_2 \exp\left(-\frac{a}{l_D}\right) \qquad (16)$$

and the force between the vesicle and membrane is given by

$$F = \frac{4\pi\,\epsilon\epsilon_0}{l_D}\varphi_1\varphi_2\,R_v\,\exp\left(-\frac{a}{l_D}\right) \qquad (17)$$

Equation (17) is plotted in Figure S3.

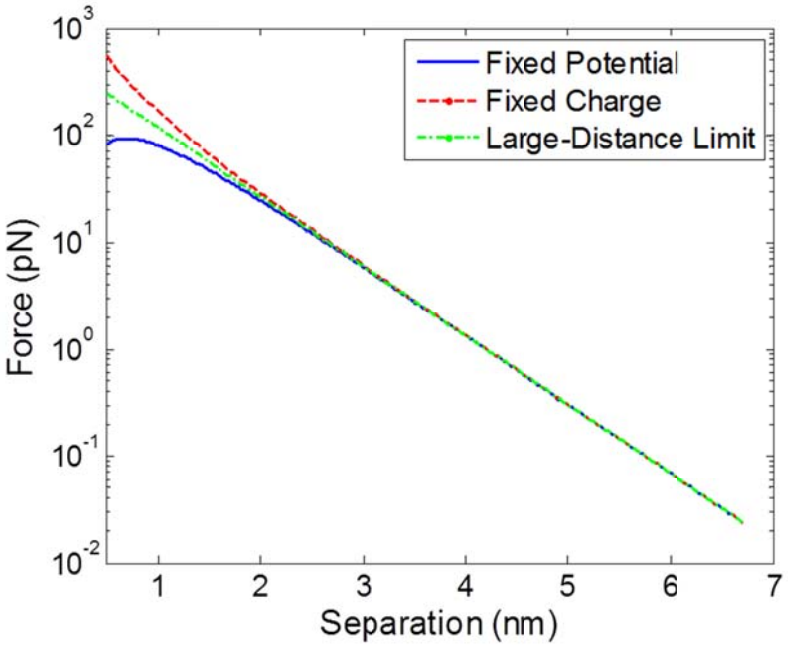

Figure S3. Distance dependence of the force produced by electrostatic repulsion between the vesicle and the membrane.

References

(1) Khripin, C.; Jagota, A.; Hui, C.-Y. *The Journal of Chemical Physics* **2005**, *123*, 134705.

(2) Maugis, D. *Contact, Adhesion and Rupture of Elastic Solids*; Springer-Verlag Berlin, 2000.

(3) Russel, W. B. and Schowalter, W. R. *Colloidal dispersions.* 1979. New York, Cambridge University Press.

(4) Alberts, B., Luis, J., Raff, M., Roberts, K., and Walter, P. Molecular *Biology of the Cell.* 2002. New Yoirk, Garland Science.

(5) Osawa H., Oshima K., and Ohki S. *Biomembranes. Biochimica et Biophysica Acta* 648, 206. 1981.

2. Relaxation of the partially unzipped SNARE complex

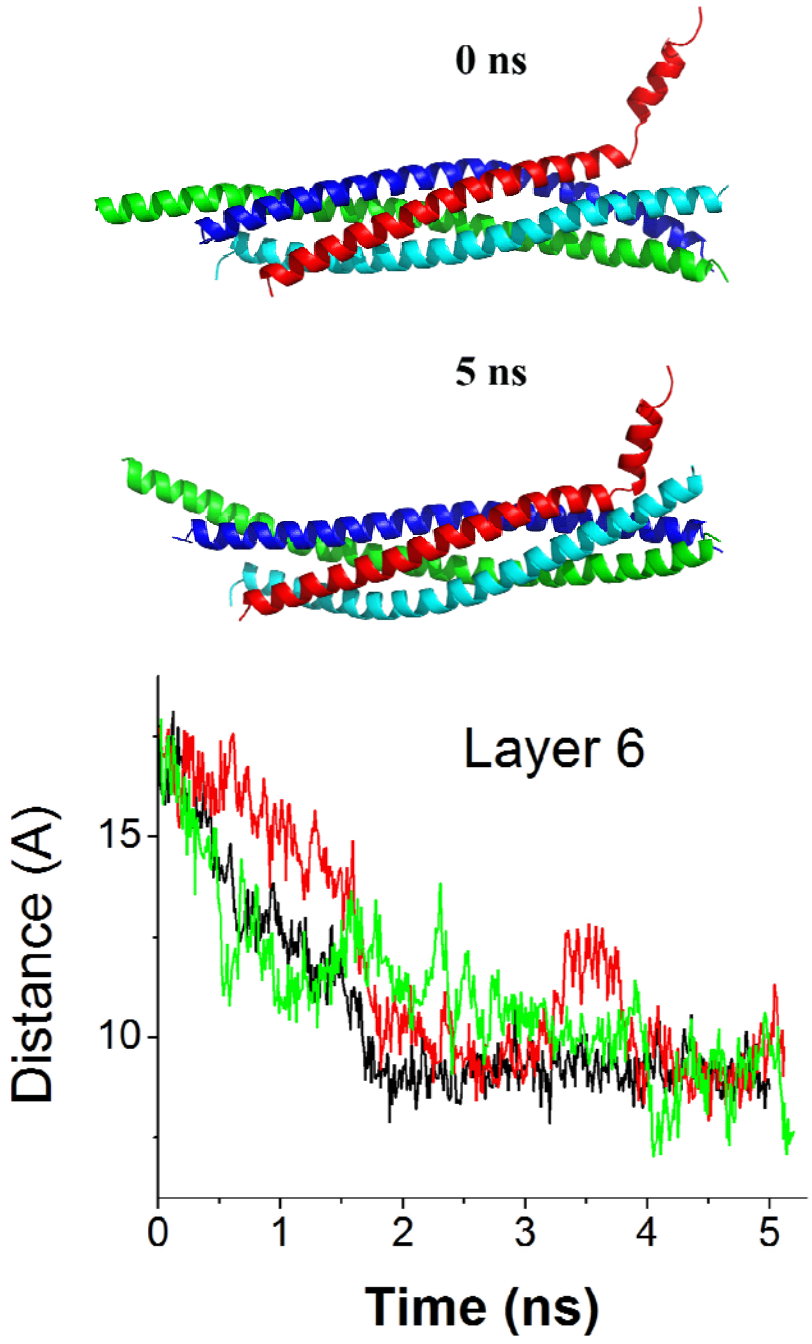

Figure S4. The SNARE conformation with layer 6 being separated from the rest of the SNARE bundle relaxes to the state with zippered layer 6 within 5 ns. Three lines (black, red, and green) correspond to three different runs. The separation of layer 6 was measured as a distance between Cα atoms of the residues F77 of Syb and A247 of Syx.

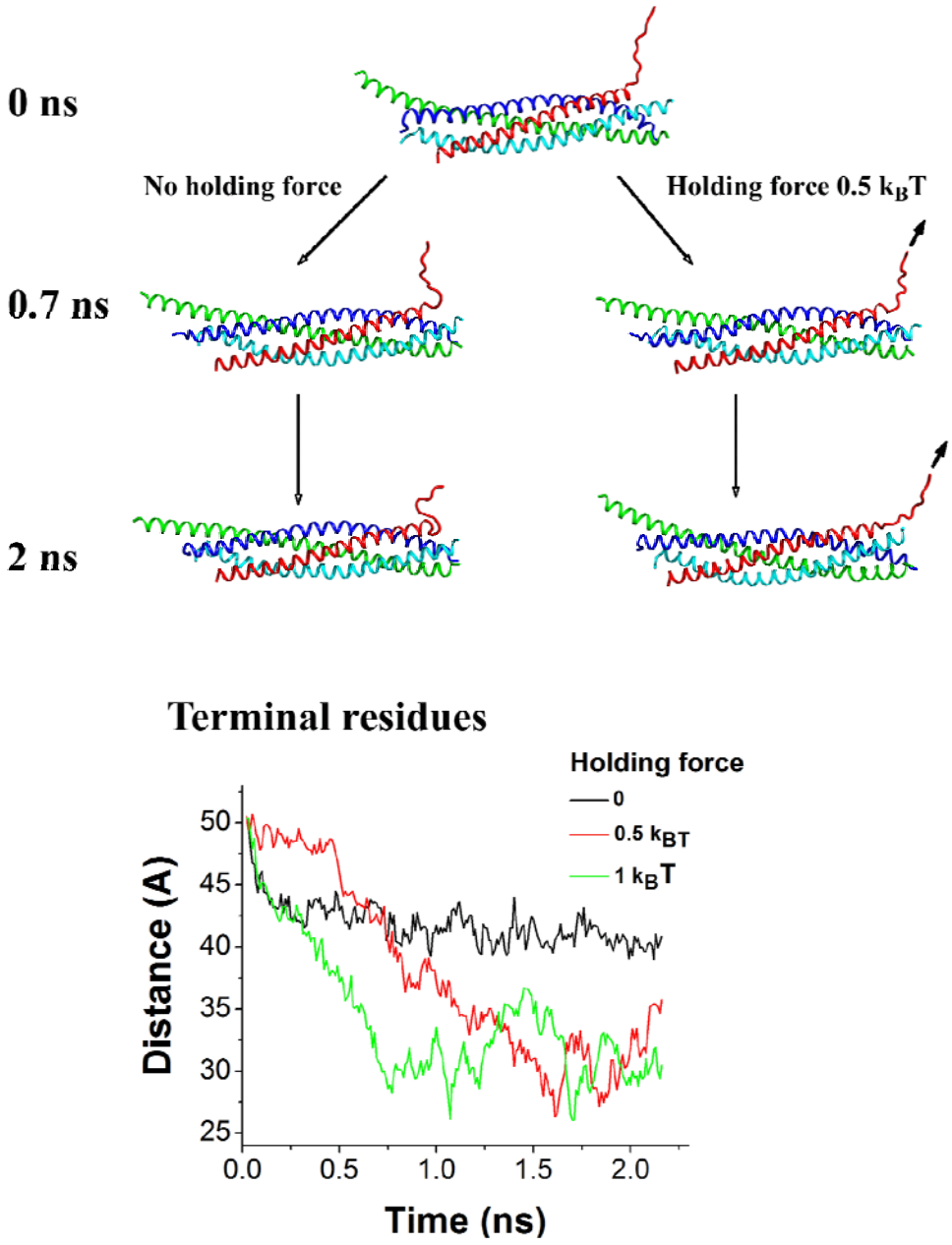

Figure S5. Holding force of 0.5-1 k_BT accelerates SNARE zippering

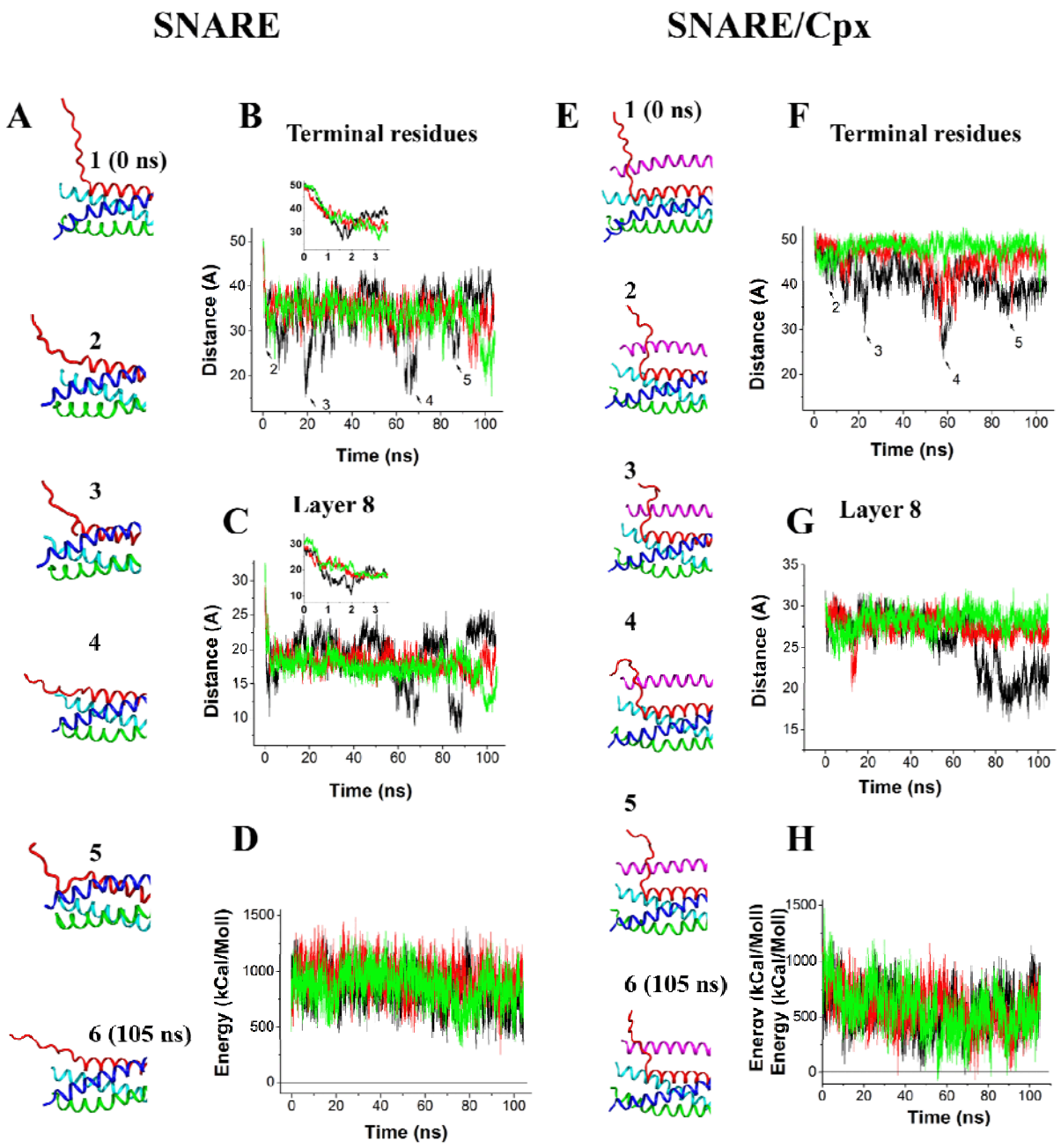

Figure S6. Relaxation of the SNARE complex without (A-D) or with (E-H) Cpx. Three independent runs are marked with different colors (black, red, green). Intermediate states (2-4, A, E) correspond to the trajectory points where the separation between Syb and Syx C-terminal residues diminishes (marked by arrows in B and F). Insets (B.C) show rapid decrease in the distance within the initial 3 ns.